A complete characterization of vibrational IR and Raman spectra of the highly-symmetrical octathia[8]circulene

Article *in* Vibrational Spectroscopy · November 2018

DOI: 10.1016/j.vibspec.2018.11.006

CITATIONS
3

READS
95

4 authors, including:

Nataliya N. Karaush
Bohdan Khmelnytsky National University of Cherkasy
32 PUBLICATIONS **293** CITATIONS
SEE PROFILE

Gleb Baryshnikov
KTH Royal Institute of Technology
153 PUBLICATIONS **1,619** CITATIONS
SEE PROFILE

Boris Minaev
Cherkasy State University, Bogdan Khmelnitskiy
396 PUBLICATIONS **5,431** CITATIONS
SEE PROFILE

Vibrational Spectroscopy 100 (2019) 107–116

Contents lists available at ScienceDirect

Vibrational Spectroscopy

journal homepage: www.elsevier.com/locate/vibspec

A complete characterization of vibrational IR and Raman spectra of the highly-symmetrical octathia[8]circulene

Valentina Minaeva[a], Nataliya Karaush-Karmazin[a,*], Gleb Baryshnikov[a,b], Boris Minaev[a]

[a] Department of Chemistry and Nanomaterials Science, Bohdan Khmelnytsky National University, 18031, Cherkasy, Ukraine
[b] Theoretical Chemistry, School of Biotechnology, Royal Institute of Technology, SE-10691, Stockholm, Sweden

ARTICLE INFO

Keywords:
Octathia[8]circulene
Tetramer
Raman spectra
FT-IR spectra
DFT calculations
Davydov splitting

ABSTRACT

The highly-symmetrical octathia[8]circulene molecule (**8S**) was synthesized and well studied 10 years ago in Moscow, including X-ray diffraction, IR and Raman spectra assignment on the ground of molecular DFT calculation. Nevertheless, this comprehensive study could not explain a big number of interesting deviations from the DFT predictions based on the molecular D_{8h} symmetry restriction being specific for a free species in a gas phase. In present work we have performed DFT optimization of the **8S** tetramer starting with the X-ray diffraction analysis of a similar crystal structure. DFT calculation of IR and Raman spectra of such a huge system provides a good assignment of the crystal-field splitting and new band occurrence. The force-field distortions, electric charges and polarizability dependence on the tetramer structure are well reproduced by the B3LYP functional with the dispersion correction. Thus, the small shifts of IR and Raman bands, their splitting and intensity redistribution upon weak intermolecular interactions in crystal packing are explained and full assignment of all observed bands is presented.

1. Introduction

The highly symmetrical architecture of a huge variety of molecular structures have long attracted chemists and set new challenges for synthetic chemistry. Vivid example of such elegance compound is a hollow and highly symmetrical C_{60} molecule which was discovered only in 1985 by laser ablation of graphite rods in an atmosphere of helium gas [1]. The possible existence of C_{60} was first predicted in 1970 [2,3] and quantum-chemical calculations of its stability and electronic structure were performed in 1973 [4]. This discovery gave rise to a new insight into the properties and behavior of sheet materials and opened up a new stage in the development of nanoscience and nanotechnology. In particular, nanotubes demonstrate a wide variety of unconventional physicochemical properties such as excellent tensile strength, high sensitivity, thermal and electrical conductivity [5–7].

Unusual highly symmetrical polyheterocyclic structure and specific electronic properties are also inherent to heterocirculenes [8–10]. Octathia[8]circulene (**8S**) represents one of the fully-heterocyclic circulene with inner planar cyclooctatetraene (COT) core (Fig. 1). This compound was synthesized by Chernichenko et. al. in 2006 through the vacuum pyrolysis of the corresponding cyclic polythiol [11]. Circulene **8S** possesses a “near planar” structure close to the D_{8h} symmetry point group according to X-ray powder diffraction analysis and ^{13}C NMR spectrometry [12,13]. It was also proposed by numerous quantum chemical calculations [14–18]. The planar structure of compound **8S** is in a good agreement with the Wynberg-Dopper's structural model based on the sector angle criterion [19].

In the solid state, the **8S** molecules are situated one under another forming the infinite columns with distances of about 3.25 Å between the neighboring molecules which are close to the distances between two neighboring atoms inside the molecule; perpendicular S···S distances are close to 3.9 Å [11]. It is interesting to note, that the **8S** single crystals have a red color that was explained by the numerous strong intermolecular S···S, S···C and C···C interactions in the crystal packing [12,19]. Such a type of crystal packing with short intermolecular contacts and π-stacking interactions provides excellent charge carrier properties (the maximum hole mobility reaches $9{\cdot}10^{-3}$ $cm^2{\cdot}V^{-1}{\cdot}s^{-1}$), as well as thermal and chemical stability that are important in modern advanced electronics, in particular for applications in organic field-effect transistors (OFETs) [14,20–26] and organic light emitting diodes (OLEDs) [27–29].

The free **8S** molecules in crystal are characterized by almost aligned C—C, C—S and C═C bond lengths in the framework of D_{8h} symmetry. The presence of the high-order symmetry axis in the studied **8S** molecule is responsible for its unique spectral properties predicted in terms of special symmetry selection rules for excitations between electronic,

* Corresponding author.
E-mail addresses: minaeva@cdu.edu.ua (V. Minaeva), karaush22@ukr.net (N. Karaush-Karmazin), glibar@kth.se (G. Baryshnikov), bfmin43@ukr.net (B. Minaev).

https://doi.org/10.1016/j.vibspec.2018.11.006
Received 18 October 2018; Received in revised form 15 November 2018; Accepted 22 November 2018
Available online 23 November 2018

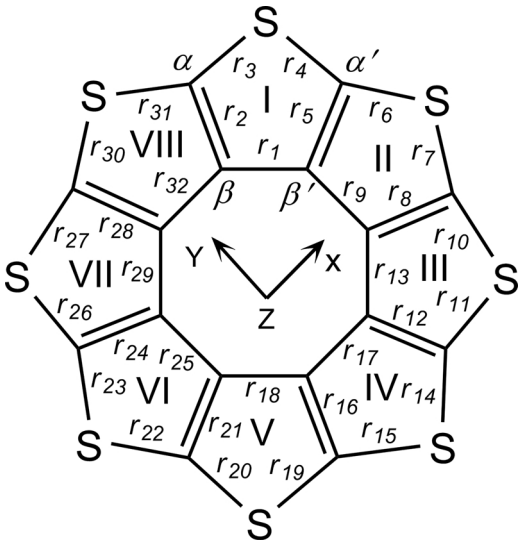

Fig. 1. The structure of the octathia[8]circulene including ring numbering, bond length classification and choice of axes used during quantum-chemical calculations.

vibrational and rotational energy levels. The most clear manifestation of the molecular symmetry role is exhibited in vibrational IR and Raman spectra of the **8S** compound detected for the first time by Bukalov et al. [12]. They have also performed the quantum-chemical explanation of some experimental data, but many vibrational features (like symmetry assignments of few normal modes, Davydov splitting phenomenon in Raman spectra and analysis of symmetry-forbidden vibrational excitations) remain unexplained so far and require more detailed theoretical study. Thus, we have performed in the current work a new analysis of the IR and Raman vibrational spectra for this highly-symmetrical octathia[8]circulene species accounting for the structural peculiarities of its monomer and its associate (tetramer) on the ground of density functional theory (DFT).

2. Computational details

The molecular structure of the studied octathia[8]circulene was optimized at the B3LYP/6–311 + + G(d,p) [30–32] DFT level [33,34] with the control of possible symmetry constrains using the Gaussian 16 package [35]. Vibrational frequencies with the corresponding IR intensities and Raman activities were calculated for the optimized geometry by the same DFT method. All vibrational frequencies were found to be real indicating that the true minimum on each total-energy hypersurface was determined. The calculated vibrational frequencies were calibrated with scaling factors to provide a direct comparison with the experimental spectra. The best coincidence of the calculated and experimental frequencies can be obtained with the scaling factor 0.987 for the 1600–100 cm^{-1} region of the spectrum. The scale factors were calculated as an averaged ratio between the experimentally observed and calculated frequencies for all lines of IR and Raman spectra of the octathia[8]circulene.

Since the calculation of the Raman line activities does not take into account the excitation energy of the molecules by laser radiation, the values of the normal vibration band activities in the Raman spectra (S_i) calculated by the DFT method were not identical to the observed scattering intensities. Therefore, the Raman activities (S_i) were recalculated into the relative Raman intensities (I_i) using the following relationship [36]:

$$I_i = \frac{f(\nu_0 - \nu_i)^4 S_i}{\nu_i\left[1 - \exp\left(-\frac{hc_0\nu_i}{kT}\right)\right]},$$

where ν_0 is the exciting laser frequency in cm^{-1} (15,805.7), ν_i is the vibrational frequency of the i-th normal mode, c, h and k are velocity of light, Planck and Boltzmann constants, respectively, f is the normalization factor.

The calculated vibrational IR and Raman spectra were plotted using the SWizard program [37] (the lines' half-width is 4 cm^{-1}) and Lorentzian distribution function.

The calculated normal vibration (NV) frequencies of the **8S** molecule do not afford to make clear assignment of many experimental weak IR and Raman bands [12]. Some of these bands are not predicted by our DFT calculations (with different basis sets) in agreement with Bukalov's DFT results (where PBE functional with SBK and 6–311 G(d) basis sets were used [12]). Since the synthesized substance **8S** was repeatedly sublimated under vacuum (10^{-5} Torr) and the finally sublimated species represented microcrystalline red needles; the studied spectra correspond to pure crystallized substance [12]. Thus, the reason for such disagreement between the measured and calculated vibrational spectra for molecule **8S** could be determined by the intermolecular perturbations in the lattice. In order to explain the occurrence of new weak lines and their splitting in experimental vibrational IR and Raman spectra we have simulated the crystal packing by calculation of tetramer structures of compound **8S**. We need to use smaller basis set (6–31 G(d)) since the tetramer calculation in the large basis set is impossible. We also introduce the dispersion correction to account for intermolecular interactions (B3LYP/GD2) [38,39]. The started atomic coordinates before geometry optimization in tetramer were obtained from X-ray diffraction analysis of the red octathia[8]circulene crystal [12]. In order to compare the calculated results for tetramer and for a single molecule we have performed additional optimization and vibrational IR and Raman spectra calculations by the same DFT approach with the same small basis set and dispersion correction GD2 (and also without it). The results are presented in Tables S1–S3 (in Supporting information).

As one can see from Tables S1 and S2 (in Supporting information) the reduction of basis set leads increase of the bond lengths and the $C^{\alpha}SC^{\alpha'}$ angle inside the thiophene fragments, but account of the dispersion correction shows a trend to relax back in some way.

Additionally, the anharmonic vibrational IR spectrum was also calculated for the **8S** monomer with the same B3LYP(GD2)/6-31G(d) method in order to compare it with the results of harmonic approximation (Table 2) and check the validity of the linear scaling approach.

3. Results and discussion

3.1. Molecular geometry of the octathia[8]circulene monomer and its tetramer

As we can see from Table S3 (and notations in Fig. 1) the structure of the **8S** compound can be discussed in terms of 17 bond lengths in the framework of the experimentally observed C_i point group for the solid samples. Moving to the putative D_{8h} point group in a gas phase the number of unequivalent bond lengths reduces to 3 (Table S3 in Supporting information). The **8S** circulene is a unique standalone molecule for which the alternation of CC bonds in the inner cyclooctatetraene (COT) core is absent (completely suppressed, Table S1) in agreement with Ref. [12]. Despite this fact, the COT core possesses the strongly antiaromatic origin, while the rest five-membered thiophene rings remain aromatic [40]. The C—S bonds (~1.74–1.76 Å) for the **8S** compounds are typically longer than the rest C—C bonds, among which the radial C—C bonds represent the shortest contacts (~1.38 Å). But accounting for numerous intermolecular interactions within the real single crystal the genuine space point group of the **8S** molecule is reduced to the lower C_i symmetry that provides more complicated vibrational spectra measured experimentally. Nevertheless, the main features of IR and Raman spectra of the free **8S** molecule are maintained in the observed bands of the crystalline red species. Actually, some symmetry forbidden normal modes within the D_{8h} point group

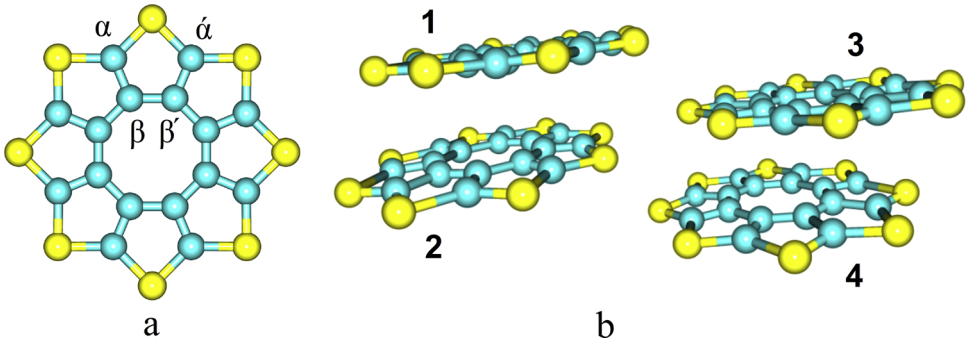

Fig. 2. The optimized structures of octathia[8]circulene (a) and its tetramer (b).

becomes formally allowed accounting inversion center as the only one possible symmetry element in the C_i point group. That is why the analysis of symmetry forbidden vibrations is a key step to a deep understanding of vibrational signals observed in the experimental spectra.

The tetramer structure was optimized without symmetry constrains (Fig. 2). Thus, even low C_i symmetry is not completely fulfilled. In agreement with the X-ray diffraction data [12] each molecule in tetramer is almost planar with small deviations of atoms from the putative plane (not more than 0.01 Å) (0.006 Å in X-ray experiment [12]). At the same time in each of the four molecules of the optimized tetramer there are no symmetry elements (Table S3 in Supporting information), though the geometry parameters are close to those of the single **8S** molecule. The largest deviation in bond lengths is recorded for the C—S bonds (0.002–0.004 Å), but the calculated tetramer C—S bond lengths are closer to the experimental values than the free molecule optimization data. The shortest intermolecular S···S contacts in the optimized tetramer is equal to 3.55 Å, while the measured S···S distances are in the range of 3.19–3.54 Å [12]. This is not a big error accounting a complicated correlation nature of intermolecular interactions and a large size of the system.

The crystal packing can be characterized in total by the following intermolecular parameters: the short S···S contacts between two columns and the longer C···C and C···S distances between two π-systems inside the column; the last are directed approximately along the crystallographic axis *a* according to the X-ray diffraction data of Ref. [12]. This supports the idea that the π-stacking coupling is definitely weaker than the S···S intermolecular interactions [12]. The approximate directions of the C–S···S–C shortened contacts are elongated in such a manner that the most of the corresponding SSC angles are close to linear structure. This is important for occurrence of particular Davydov-type splitting of vibrational bands [41].

3.2. Vibrational spectra of the octathia[8]circulene molecules and tetramer

The vibrational spectrum of **8S** molecule, which consists of 24 atoms, contains 66 normal vibration modes. General assignment of normal vibrations according symmetry species in the D_{8h} symmetry point group, their mutual correlation and selection rules for activity in IR and Raman spectra are presented in Table 1.

As one can see from Table S3 (in Supporting information) the reduction of the basis set does not influence significantly the normal vibrations frequency and intensity of the **8S** molecule in the range below 1300 см$^{-1}$, excluding non-active vibrations in IR and Raman spectra $\nu_{34(33)}$ e_{3g}, $\nu_{32(31)}$ e_{2u}, ν_{30} b_{2u}, and also NVs $\nu_{11(10)}$ e_{3g} and $\nu_{29(28)}$ e_{1g}. These modes belong to the out-of-plane deformations of thiophene fragments and COT. The reduction of basis set also leads to frequency increase of vibrations determined by the bond stretching modes of the thiophene's fragments (region 1600–1300 см$^{-1}$) which is connected with the obvious changes in the bond lengths (Table S3 in Supporting information).

In the tetramer counterparts molecules the form of normal vibrations remains almost the same and occurs in each molecule one by one in turn. Small deviations of the structural parameters of molecules in tetramer from those in single molecule immediately leads to the eight-fold splitting of the former degenerate modes and to the four-fold splitting of the former non-degenerate vibrations (Tables 2 and 3). A complete list of all normal vibrations is given in Table S5 (in Supporting information).

Table 1
Type and symmetry of normal vibrations and their activity selection rules in the D_{8h} symmetry point group.

D_{8h}[a]			In-plane/ out-of-plane normal vibration
Symmetry[b]	Method		
	IR	Raman	
e_{1u} (5 × 2)	+	–	in-plane
e_{3u} (6 × 2)	–	–	in-plane
e_{1g} (2 × 2)	–	+	out-of-plane
e_{3g} (3 × 2)	–	–	out-of-plane
a_{2u} (2)	+	–	out-of-plane
b_{1u} (1)	–	–	out-of-plane
b_{2g} (3)	–	–	in-plane
a_{1g} (3)	–	+	in-plane
e_{2g} (3 × 2)	–	+	in-plane
e_{2g} (3 × 2)	–	+	in-plane
a_{1u} (0)	–	–	out-of-plane
b_{2u} (2)	–	–	out-of-plane
e_{2u} (3 × 2)	–	–	out-of-plane
b_{1g} (3)	–	–	in-plane
a_{2g} (2)	–	–	in-plane

[a] Notation of axes is given in Fig. 1.
[b] The numbers of vibrational modes of the given symmetry type are presented in parentheses.

In the absence of D_{8h} symmetry in tetramer, all vibrations are allowed in the IR and Raman spectra and some normal vibrations provide additional weak bands in the observed experimental spectra. In the low-frequency range (less than 200 см$^{-1}$) we observe mixing of few types of vibrations i.e. in the separate molecules of tetramer one can see mixing of different vibration types.

Below 80 см$^{-1}$ in the tetramer vibrational spectra we have calculated new modes of translation and libration types. Among them in the Raman spectrum there are lines 44 and 77 см$^{-1}$ with the calculated activity of 35 and 11 Å^4/amu, respectively. The first line is assigned to libration's mode and the second – to translational type of intermolecular vibration.

3.2.1. IR spectra of the octathia[8]circulene molecule and tetramer

In the framework of D_{8h} symmetry only two a_{2u} modes and the doubly degenerate e_{1u} (five modes) normal vibrations are IR active according to electric-dipole selection rules; thus, only seven frequency bands (2 + 5, Table 1) may appear in the IR spectrum of the **8S** molecule. The most intense band in IR spectrum of **8S** molecule at

Table 2
The IR spectrum of the octathia[8]circulene molecule (D_{8h} symmetry) and its tetramer splitting calculated by the B3LYP GD2/6-31 G(d) method and assignment of the calculated normal vibrations in the tetramer (with account of scaling factor 0.987).

Molecule **8S**					Tetramer		Freq. exp.	Assignment
Mode	Freq. cal. (harm)	I_{IR} (harm)	Freq. cal. (anharm)	I_{IR} (anharm)	Freq. cal.	I_{IR}		
ν_{58} e_{1u}	1424	24	1409	22	1425.3	38.2	**1405**	$C^{\alpha}C^{\beta}$ and $C^{\alpha'}C^{\beta'}$ str., s., IV, VIII out-of-phase
					1425.3	18.3		
					1424.5	16.2		
					1424.3	4.7		
ν_{57} e_{1u}	1424	24	1409	22	1424.2	0.3	**1405**	$C^{\alpha}C^{\beta}$ and $C^{\alpha'}C^{\beta'}$ str., s., II ,VI out-of-phase
					1424.1	43.8		
					1424.0	4.0		
					1423.8	11.8		
ν_{56} a_{1g}	1422	–	1408	–	1422.5	0.7	**1405**	$C^{\alpha}C^{\beta}$ and $C^{\alpha'}C^{\beta'}$ str., s., I–VIII in phase
					1422.4	0.1		
					1421.2	20.2		
					1421.1	2.3		
ν_{53} e_{1u}	1118	1.2	1111	1.0	1119.8	1.5	**1110**	$C^{\alpha}S$ and $C^{\alpha'}S$ str., s., $C^{\beta}C^{\beta'}$ str., III, VII out-of-phase
					1119.6	1.7		
					1119.2	1.0		
					1119.1	2.8		
ν_{52} e_{1u}	1118	1.2	1111	1.0	1118.6	0.6	**1110**	$C^{\alpha}S$ and $C^{\alpha'}S$ str., s., $C^{\beta}C^{\beta'}$ str., I, V out-of-phase
					1118.5	0.1		
					1118.4	0.01		
					1118.1	0.01		
ν_{50} e_{3u}	1033	–	1025	0.03	1039.0	2.7	**1037**	$C^{\alpha}S$ and $C^{\alpha'}S$ str., s., II, IV, VII and III, VI, VIII out-of-phase, $C^{\alpha}S$ and $C^{\alpha'}S$ str., as., I, V
					1038.2	0.4		
					1037.5	1.6		
					1037.3	1.4		
ν_{49} e_{3u}	1033	–	1025	0.03	1035.8	0.1	**1037**	$C^{\alpha}S$ and $C^{\alpha'}S$ str., s., I, IV, VI and II, V, VII out-of-phase, $C^{\alpha}S$ and $C^{\alpha'}S$ str., as., III, VII
					1035.6	0.03		
					1035.3	0.03		
					1035.2	0.1		
ν_{47} e_{2g}	998	–	992	–	1002.8	2.1	**979/**	$C^{\alpha}SC^{\alpha'}$ bend. II, VI and IV, VIII out-of-phase, $C^{\alpha}S$ and $C^{\alpha'}S$ str., as. I, III, V, VII
					1002.6	0.03	**994**	
					1002.0	4.9		
					1001.8	0.2		
ν_{46} e_{2g}	998	–	992	–	1000.3	0.03	**979/**	$C^{\alpha}SC^{\alpha'}$ bend. I, V and III, VII out-of-phase, $C^{\alpha}S$ and $C^{\alpha'}S$ str., as. II, IV, VI, VIII
					1000.0	0.3	**994**	
					999.8	0.03		
					999.7	0.4		
ν_{45} e_{1u}	948	86	938	74	951.7	159.3	**958**	$C^{\alpha}S$ and $C^{\alpha'}S$ str., as., II, III, IV, VI, VII, VIII, $C^{\alpha}SC^{\alpha'}$ bend., I and V out-of-phase
					951.0	54.0		
					960.4	26.3		
					950.0	234.0		
ν_{44} e_{1u}	948	86	938	74	949.8	61.3	**948**	$C^{\alpha}S$ and $C^{\alpha'}S$ str., as., VIII, I, II, IV, V, VI, $C^{\alpha}SC^{\alpha'}$ bend., III and VII out-of-phase
					949.3	8.9		
					948.7	1.3		
					948.4	0.1		
ν_{42} b_{1g}	800	–	796	–	800.4	0.001	**797**	Def. as. in COT, in-plane
					800.4	0.06		
					800.2	0.03		
					800.1	0.06		
ν_{41} e_{3u}	721	–	715	–	721.7	0.02	**726**	Def. as. III, VII
					721.6	0.1		
					721.5	0.03		
					721.5	0.004		
ν_{40} e_{3u}	721	–	715	–	721.4	0.03	**726**	Def. as. I, V
					721.3	0.02		
					721.2	0.01		
					721.2	0.02		
ν_{35} e_{1u}	649	0.02	648	–	651.0	1.3	**657**	$C^{\alpha}S$ and $C^{\alpha'}S$ str., s., $C^{\alpha}SC^{\alpha'}$ bend., III and VII out-of-phase
					650.6	0.8		
					650.6	0.4		
					650.5	0.9		
ν_{34} e_{1u}	649	0.02	648	–	649.6	0.03	**651**	$C^{\alpha}S$ and $C^{\alpha'}S$ str., s., $C^{\alpha}SC^{\alpha'}$ bend., I and V out-of-phase
					649.0	0.3		
					648.4	0.03		
					648.3	0.01		
ν_{27} a_{2u}	502	22	505	21	501.8	0.8	**500**	COT out-of-plane, def. I–VIII, out-of-plane, in-phase
					501.3	0.03		
					500.1	2.6		
					499.9	111.1		

(*continued on next page*)

Table 2 (*continued*)

Molecule **8S**					Tetramer		Freq. exp.	Assignment
Mode	Freq. cal. (harm)	I_{IR} (harm)	Freq. cal. (anharm)	I_{IR} (anharm)	Freq. cal.	I_{IR}		
ν_{17} e_{1u}	278	3	271	2	281.9	0.07	**278**	Rocking of heterocycle, II, III, IV and VI, VII, VIII, in-plane
					281.2	2.2		
					281.0	0.5		
					280.9	2.1		
ν_{16} e_{1u}	278	3	271	2	280.6	4.4	**278**	Rocking of heterocycle, VIII, I, II and V, VI,VII, in-plane
					280.5	2.2		
					280.0	6.3		
					279.9	0.2		

Freq., frequency (cm^{-1}); I_{IR}, IR intensity (km/mol); cal., calculated; exp., experimental; def., deformation; s, symmetric; as, asymmetric; I, II, III, IV, V, VI, VII, VIII, heterocycle numbers (see Fig. 1); bend., bending; str., stretching; COT, cyclooctatetraene.

948 cm^{-1} (Fig. 3, curve 2) is formed by degenerate normal modes ν_{45} and ν_{44} of the e_{1u} symmetry (Table 2); they belong to asymmetric stretching vibrations of the C—S bonds which are mixed with the bending vibrations of the $C^{\alpha}SC^{\alpha'}$ angle. In the observed IR spectrum (Fig. 3, curve 1) this band is split and shows two peaks at 948 (958) cm^{-1} of different intensity. This can be explained on the ground of the tetramer calculation; however, the calculated spitting (3.3 cm^{-1}) is not so big in comparison with the experiment (10 cm^{-1}). Each mode, ν_{45} and ν_{44}, has its own small splitting (about 1.4 cm^{-1}) and particular intensity distribution (Table 2) but the FTIR spectrometer can not afford such high resolution and these hyperfine structure details. Anyway, our B3LYP GD2 calculations reproduce the blue shift and large intensity difference of two main components of the split band.

The symmetric stretching vibrations of the C—S bonds ($\nu_{53(52)}$, $\nu_{35(34)}$) are predicted with low intensity in the DFT calculated IR spectrum of the **8S** molecule, but experimental IR absorption of the red crystal of the octathia[8]circulene compound (Fig. 3, curve 1) exhibits the split band $\nu_{35(34)}$ at 657(651) cm^{-1} of middle intensity. The calculated IR spectrum of tetramer indicates that this band will be split and its absorption intensity will increase (with more intense high-frequency component; Fig. 3, curve 3; Table 2).

Degenerate vibrations $\nu_{58(57)}$ of e_{1u} symmetry produce the middle intensity band of symmetric $C^{\alpha}C^{\beta}$ and $C^{\alpha'}C^{\beta'}$ stretching vibrations with the calculated 1424 cm^{-1} and experimental 1405 cm^{-1} frequencies. In the large basis set (B3LYP/6-311++G(d,p) this band is predicted at 1407 cm^{-1} (Table S4 in Supporting information). This band can overlap a close lying band at 1422 cm^{-1} (Table 2), which belongs to a_{1g} symmetry and refers to symmetric $C^{\alpha}C^{\beta}$ and $C^{\alpha'}C^{\beta'}$ stretching vibrations; but they take place in phase inside **8S** molecule (NV ν_{56}). Vibration ν_{56} of the a_{1g} symmetry is forbidden in IR spectrum of molecule **8S**, but allowed in IR spectrum of tetramer and exhibits the middle intensity (20.2 km/mol). One should note that NV ν_{56} of the a_{1g} symmetry is the most active vibration in the Raman spectrum of molecule **8S**.

The strong band in experimental IR spectrum of the **8S** compound at 500 cm^{-1} (Fig. 3, curve 1) belongs to the out-of-plane vibrations of the central COT core; in the calculated IR spectrum of this molecule (ν_{27} of the a_{2u} symmetry, Table 2) the corresponding band with a frequency 502 cm^{-1} provides rather moderate intensity. But in the IR spectrum of tetramer the intensity of this band is increased suddenly and reaches a high value of 111 km/mol (just for the low-frequency component, Table 2). This is in a good agreement with experiment [12] and with an obvious underestimation of this band intensity in the single molecule calculation, Fig. 3 (see also Fig. 6 in Ref. [12]).

A weak band at 278 cm^{-1} which corresponds to the planar rocking vibrations of the thiophene fragments (NV $\nu_{17(16)}$ of e_{1u} symmetry, Table 2) has the same frequency in the observed IR spectrum. But its intensity in the calculated tetramer is three times enhanced in a good agreement with observation [12] (Fig. 3, curves 3 and 1).

We have assigned the experimental weak band 1037 cm^{-1} to the stretching vibration of C—S bonds. In IR spectrum of the free **8S** molecule this band is forbidden by symmetry ($\nu_{50(49)}$ e_{3u} symmetry, Table 2). But it becomes allowed in the tetramer IR spectrum, though it provides a very weak band (Table 2). Together with the IR forbidden band 1033 cm^{-1} (Table 2) which is slightly split (0.6 cm^{-1}) and enhanced in the calculated tetramer all these bands system reproduces pretty well the weak fine-structure features around 1037 cm^{-1} in the experimental IR spectrum (Fig. 3, curve 1) [12].

There are also very weak experimental IR bands 797 and 726 cm^{-1} (Fig. 3) which could be produced by vibration modes ν_{42} of b_{1g} symmetry and $\nu_{41(40)}$ of e_{3u} symmetry, respectively, in the calculated IR spectrum of tetramer. The low intensity of these bands is in a qualitative agreement with experimental measurements [12] (Table 2, Fig. 3).

A wide weak band with a maximum at 979 cm^{-1} and a right shoulder at 994 cm^{-1} (Fig. 3, curve 1) can be assigned to the CSC bending vibrations (Table 2). In IR spectrum of the free **8S** molecule this corresponds to normal mode $\nu_{47(46)}$ of the e_{2g} symmetry with the calculated frequency 998 cm^{-1}, which is allowed only in Raman spectrum of the **8S** molecule. In the calculated IR spectrum of tetramer this type of vibrations becomes allowed and provides a bands system with a maximum at 1002 cm^{-1} (Table 2, Fig. 3, curve 3).

In the experimental IR spectrum of the **8S** compound, taken from Ref. [12], there are also two weak bands at 1345 and 864 cm^{-1}, which are absent in the calculated IR spectra of the **8S** molecule and of its tetramer; this is most likely due to insufficient purification of the sample.

Account of anharmonicity for the calculated frequencies and intensities in the IR absorption spectrum of the **8S** molecule provides the results which are more close to experimental values (Table 2, Fig. S1 in Supporting information) than the unscaled DFT predictions. The anharmonic approach gives a reasonable support to the scale factors widely used in our previous DFT calculations of various hetero[8]circulenes vibrational spectra [8,10,17]. Calculation of all important overtones predicts zero IR intensity but a big number of combination bands are calculated with observable activity (Table S6 in Supporting Information). Meanwhile, all of them are overlapped by the principal 0-1 intense transitions. We assume that the pairs of combination modes ν_{51}, ν_{29} and ν_{50}, ν_{29} with energy 980 cm^{-1} and intensity of 6.24 km·mol^{-1} (Table S6) contribute to the band observed at 979 cm^{-1}in the experimental IR spectrum of the **8S** compound (Fig. 3).

3.2.2. *Raman spectra of the octathia[8]circulene molecule and its tetramer*

For the D_{8h} symmetry only totally symmetric modes of the a_{1g} species and doubly degenerate e_{1g} and e_{2g} modes are Raman-active (Table 1). Thus, the Raman spectrum of the free molecule **8S** may exhibit 11 lines. The calculated and experimental Raman spectra are presented in Fig. 4. Raman spectra are given for two modifications (red and white) of the solid sample [12]. Both are obtained under gradual sublimation and represent microcrystalline and amorphous parts of the

Table 3
Calculated Raman spectrum of the octathia[8]circulene molecule (D_{8h} symmetry) and its tetramer splitting by the B3LYP GD2/6-31 G(d) method and assignment of calculated normal vibrations in the tetramer (with account of scaling factor 0.987).

Molecule 8S				Tetramer			Freq. exp.	Assignment
Mode	Freq. cal.	S_i	I_R	Freq. cal.	S_i	I_R		
ν_{65} e_{3u}	1587	–	–	1590.4	1.8	$1.7{\cdot}10^{-3}$	1594	$C^{\beta}C^{\beta'}$ str., I, V out-of-phase
				1590.3	6.1	$5.8{\cdot}10^{-3}$		
				1590.0	2.7	$2.6{\cdot}10^{-3}$		
				1589.9	2.2	$2.1{\cdot}10^{-3}$		
ν_{64} e_{3u}	1587	–	–	1589.8	2.8	$2.7{\cdot}10^{-3}$	1594	$C^{\beta}C^{\beta'}$ str., III, VII out-of-phase
				1589.3	5.6	$5.3{\cdot}10^{-3}$		
				1589.1	2.6	$2.5{\cdot}10^{-3}$		
				1588.8	3.3	$3.1{\cdot}10^{-3}$		
ν_{62} e_{2g}	1487	242	$3.0{\cdot}10^{-1}$	1488.6	222.6	$2.3{\cdot}10^{-1}$	1480	$C^{\beta}C^{\beta'}$str. I, V and III, VII out-of-phase
				1488.6	94.5	$9.8{\cdot}10^{-2}$		
				1488.2	195.6	$2.0{\cdot}10^{-1}$		
				1488.1	202.1	$2.1{\cdot}10^{-1}$		
ν_{61} e_{2g}	1487	242	$3.0{\cdot}10^{-1}$	1488.1	153.2	$1.6{\cdot}10^{-1}$	1480	$C^{\beta}C^{\beta'}$ str. II, VI and IV, VIII out-of-phase
				1487.7	100.6	$1.0{\cdot}10^{-1}$		
				1488.7	171.9	$1.8{\cdot}10^{-1}$		
				1487.5	139.8	$1.5{\cdot}10^{-1}$		
ν_{56} a_{1g}	1422	705	1.0	1422.5	83.2	$9.2{\cdot}10^{-2}$	1403	$C^{\alpha}C^{\beta}$ and $C^{\alpha'}C^{\beta'}$ str., s., I–VIII
				1422.4	400.5	$4.4{\cdot}10^{-1}$		
				1421.2	9.7	$1.1{\cdot}10^{-2}$		
				1421.1	110.5	$1.2{\cdot}10^{-1}$		
ν_{55} e_{2g}	1314	17	$3.0{\cdot}10^{-2}$	1315.0	40.3	$5.0{\cdot}10^{-2}$	1295	$C^{\alpha}C^{\beta}$ and $C^{\alpha'}C^{\beta'}$ str., s., $C^{\beta}C^{\beta'}$ str., $C^{\alpha}SC^{\alpha'}$ bend. II, VI and IV, VIII out-of-phase
				1314.9	3.5	$4.3{\cdot}10^{-3}$		
				1314.7	3.7	$4.6{\cdot}10^{-3}$		
				1314.6	37.1	$4.6{\cdot}10^{-2}$		
ν_{54} e_{2g}	1314	17	$3.0{\cdot}10^{-2}$	1314.3	1.9	$2.4{\cdot}10^{-3}$	1295	$C^{\alpha}C^{\beta}$ and $C^{\alpha'}C^{\beta'}$ str., s., $C^{\beta}C^{\beta'}$ str., $C^{\alpha}SC^{\alpha'}$ bend. I, V and III, VII out-of-phase
				1314.2	1.0	$1.2{\cdot}10^{-3}$		
				1314.1	2.2	$2.7{\cdot}10^{-3}$		
				1313.9	3.6	$4.5{\cdot}10^{-3}$		
ν_{51} b_{2g}	1053	–	–	1058.9	0.1	$1.7{\cdot}10^{-4}$	1056	$C^{\alpha}S$ and $C^{\alpha'}S$ str., s. I, III, V, VII and II, IV, VI, VIII out-of-phase
				1058.4	0.5	$8.3{\cdot}10^{-4}$		
				1054.0	0.4	$6.7{\cdot}10^{-4}$		
				1053.7	0.003	$5.0{\cdot}10^{-6}$		
ν_{50} e_{3u}	1033	–	–	1039.0	0.4	$6.8{\cdot}10^{-4}$	1039	$C^{\alpha}S$ and $C^{\alpha'}S$ str., s., II, IV, VII and III, VI, VIII out-of-phase, $C^{\alpha}S$ and $C^{\alpha'}S$ str., as., I, V
				1038.2	2.0	$3.4{\cdot}10^{-3}$		
				1037.5	0.4	$6.8{\cdot}10^{-4}$		
				1037.3	0.06	$1.0{\cdot}10^{-4}$		
ν_{49} e_{3u}	1033	–	–	1035.8	0.1	$1.7{\cdot}10^{-4}$	1039	$C^{\alpha}S$ and $C^{\alpha'}S$ str., s., I, IV, VI and II, V, VII out-of-phase, $C^{\alpha}S$ and $C^{\alpha'}S$ str., as., III, VII
				1035.6	0.01	$1.7{\cdot}10^{-5}$		
				1035.3	0.05	$8.5{\cdot}10^{-5}$		
				1035.2	0.07	$1.2{\cdot}10^{-4}$		
ν_{47} e_{2g}	998	6	$1.0{\cdot}10^{-2}$	1002.8	0.8	$1.4{\cdot}10^{-3}$	1003	$C^{\alpha}SC^{\alpha'}$ bend. II, VI and IV, VIII out-of-phase, $C^{\alpha}S$ and $C^{\alpha'}S$ str., as. I, III, V, VII
				1002.6	29.4	$5.2{\cdot}10^{-2}$		
				1002.0	0.4	$7.1{\cdot}10^{-4}$		
				1001.8	14.7	$2.6{\cdot}10^{-2}$		
ν_{46} e_{2g}	998	6	$1.0{\cdot}10^{-2}$	1000.3	0.1	$1.8{\cdot}10^{-4}$	1003	$C^{\alpha}SC^{\alpha'}$ bend. I, V and III, VII out-of-phase, $C^{\alpha}S$ and $C^{\alpha'}S$ str., as. II, IV, VI, VIII
				1000.0	0.1	$1.8{\cdot}10^{-4}$		
				999.8	1.3	$2.3{\cdot}10^{-3}$		
				999.7	0.1	$1.8{\cdot}10^{-4}$		
ν_{43} a_{1g}	832	31	$9.0{\cdot}10^{-2}$	833.3	7.6	$1.7{\cdot}10^{-2}$	829	Breathing COT
				833.1	120.0	$2.7{\cdot}10^{-1}$		
				832.2	5.8	$1.3{\cdot}10^{-2}$		
				831.9	1.0	$2.3{\cdot}10^{-3}$		
ν_{42} b_{1g}	800	–	–	800.4	0.07	$1.7{\cdot}10^{-4}$	806 w	Def. as. COT, in-plane
				800.4	0.005	$1.2{\cdot}10^{-5}$		
				800.2	0.01	$2.4{\cdot}10^{-5}$		
				800.1	0.05	$1.2{\cdot}10^{-4}$		
ν_{37} e_{3g}	684	–	–	682.7	0.1	$2.9{\cdot}10^{-4}$	698	Def. as. I, V, out-of-plane
				682.7	0.07	$2.1{\cdot}10^{-4}$		
				682.2	0.2	$5.9{\cdot}10^{-4}$		
				682.1	0.17	$5.0{\cdot}10^{-4}$		
ν_{36} e_{3g}	684	–	–	682.1	0.15	$4.4{\cdot}10^{-4}$	698	Def. as. III, VII, out-of-plane
				681.9	0.05	$1.5{\cdot}10^{-4}$		
				681.9	0.4	$1.2{\cdot}10^{-3}$		
				681.7	0.1	$2.9{\cdot}10^{-4}$		
ν_{33} e_{2g}	626	24	$1.0{\cdot}10^{-1}$	628.3	41.3	$1.4{\cdot}10^{-1}$	631	Def. as. COT, in-plane, $C^{\alpha}SC^{\alpha'}$ bend II, VI and IV, VIII out-of-phase
				628.0	41.7	$1.4{\cdot}10^{-1}$		
				627.9	33.5	$1.1{\cdot}10^{-1}$		
				627.8	42.1	$1.4{\cdot}10^{-1}$		

(*continued on next page*)

Table 3 (*continued*)

Molecule 8S				Tetramer			Freq. exp.	Assignment
Mode	Freq. cal.	S_i	I_R	Freq. cal.	S_i	I_R		
ν_{32} e_{2g}	626	24	$1.0{\cdot}10^{-1}$	627.6	1.3	$4.3{\cdot}10^{-3}$	628	Def. as. COT, in-plane, $C^{\alpha}SC^{\alpha\prime}$ bend I, V and III, VII out-of-phase
				627.4	1.2	$3.9{\cdot}10^{-3}$		
				627.3	0.4	$1.3{\cdot}10^{-3}$		
				627.2	0.7	$2.3{\cdot}10^{-3}$		
ν_{29} e_{1g}	518	1.6	$9.0{\cdot}10^{-3}$	518.4	0.02	$8.5{\cdot}10^{-5}$	518	I, V waving, out-of-phase, out-of-plane
				518.3	0.06	$2.5{\cdot}10^{-4}$		
				517.3	0.6	$2.5{\cdot}10^{-3}$		
				517.1	3.3	$1.4{\cdot}10^{-2}$		
ν_{28} e_{1g}	518	1.6	$9.0{\cdot}10^{-3}$	516.9	1.0	$4.2{\cdot}10^{-3}$	518	III, VII waving, out-of-phase, out-of-plane
				516.7	0.5	$2.1{\cdot}10^{-3}$		
				515.8	9.9	$4.2{\cdot}10^{-2}$		
				515.3	0.7	$3.0{\cdot}10^{-3}$		
ν_{26} b_{2g}	428	–	–	429.7	1.7	$9.3{\cdot}10^{-3}$	430	$C^{\alpha}SC^{\alpha\prime}$ bend I, III, V, VII and II, IV, VI, VIII, out-of-phase
				429.3	1.6	$8.8{\cdot}10^{-3}$		
				429.2	0.5	$2.7{\cdot}10^{-3}$		
				429.1	0.1	$5.5{\cdot}10^{-4}$		
ν_{25} b_{1g}	417	–	–	420.0	4.7	$2.7{\cdot}10^{-2}$	420	Rocking of heteroatom, I–VIII, in-plane
				419.8	0.3	$1.7{\cdot}10^{-3}$		
				419.0	0.06	$3.4{\cdot}10^{-4}$		
				418.9	4.6	$2.6{\cdot}10^{-2}$		
ν_{24} e_{3u}	416	–	–	417.4	2.8	$1.6{\cdot}10^{-2}$	417	$C^{\alpha}SC^{\alpha\prime}$ bend I, V, out-of-phase
				416.9	3.0	$1.7{\cdot}10^{-2}$		
				416.7	0.95	$5.4{\cdot}10^{-3}$		
				416.6	0.2	$1.1{\cdot}10^{-3}$		
ν_{23} e_{3u}	416	–	–	416.2	0.1	$5.7{\cdot}10^{-4}$	417	$C^{\alpha}SC^{\alpha\prime}$ bend III, VII, out-of-phase
				416.1	0.2	$1.1{\cdot}10^{-3}$		
				416.0	0.01	$5.7{\cdot}10^{-5}$		
				416.0	0.2	$1.1{\cdot}10^{-3}$		
ν_{20} a_{1g}	337	44	$4.0{\cdot}10^{-1}$	339.5	129.7	1.0	345	Breathing of macrocycle
				339.1	19.0	$1.5{\cdot}10^{-1}$		
				338.8	22.2	$1.7{\cdot}10^{-1}$		
				338.7	8.9	$6.9{\cdot}10^{-2}$		
ν_{19} e_{2g}	336	10	$1.0{\cdot}10^{-1}$	338.5	17.0	$1.3{\cdot}10^{-1}$	338	Rocking of heteroatom, I, III, V, VII, in-plane
				338.1	12.0	$9.3{\cdot}10^{-2}$		
				337.9	23.0	$1.8{\cdot}10^{-1}$		
				337.5	0.8	$6.2{\cdot}10^{-3}$		
ν_{18} e_{2g}	336	10	$1.0{\cdot}10^{-1}$	337.3	5.3	$4.1{\cdot}10^{-2}$	338	Rocking of heteroatom, II, IV, VI, VIII, in-plane
				337.2	2.2	$1.7{\cdot}10^{-2}$		
				337.2	7.6	$5.9{\cdot}10^{-2}$		
				336.9	0.06	$4.7{\cdot}10^{-4}$		
ν_{15} e_{2u}	264	–	–	272.9	0.1	$1.1{\cdot}10^{-3}$	275	II, IV, VI, VIII waving, out-of-plane
				272.8	0.4	$4.3{\cdot}10^{-3}$		
				272.3	0.6	$6.5{\cdot}10^{-3}$		
				272.1	0.2	$2.2{\cdot}10^{-3}$		
ν_{14} e_{2u}	264	–	–	271.2	0.2	$2.2{\cdot}10^{-3}$	275	I, III, V, VII waving, out-of-plane
				271.0	0.2	$2.2{\cdot}10^{-3}$		
				269.6	1.2	$1.3{\cdot}10^{-2}$		
				269.5	0.7	$7.7{\cdot}10^{-3}$		
ν_{13} e_{2g}	249	8	$1.0{\cdot}10^{-1}$	250.4	0.3	$3.7{\cdot}10^{-3}$	255	Def. COT, as., in-plane
				250.4	3.6	$4.4{\cdot}10^{-2}$		
				250.0	30.3	$3.7{\cdot}10^{-1}$		
				249.8	1.4	$1.7{\cdot}10^{-2}$		
ν_{12} e_{2g}	249	8	$1.0{\cdot}10^{-1}$	249.4	0.07	$8.7{\cdot}10^{-4}$	251	Def. COT, as., in-plane
				249.3	1.7	$2.1{\cdot}10^{-2}$		
				249.0	14.0	$1.7{\cdot}10^{-1}$		
				248.9	1.0	$1.2{\cdot}10^{-2}$		
ν_{9} e_{1g}	219	2	$4.0{\cdot}10^{-2}$	227.8	0.1	$1.4{\cdot}10^{-3}$	222	III, VII waving, out-of-phase, out-of-plane
				227.7	0.03	$4.3{\cdot}10^{-4}$		
				227.2	0.06	$8.6{\cdot}10^{-4}$		
				226.6	0.2	$2.9{\cdot}10^{-3}$		
ν_{8} e_{1g}	219	2	$4.0{\cdot}10^{-2}$	224.9	15.0	$2.2{\cdot}10^{-1}$	222	I, V waving, out-of-phase, out-of-plane
				224.4	1.5	$2.2{\cdot}10^{-2}$		
				222.1	1.7	$2.5{\cdot}10^{-2}$		
				221.9	4.2	$6.3{\cdot}10^{-2}$		
ν_{6} b_{1u}	169	–	–	179.3	0.03	$6.3{\cdot}10^{-4}$	164	Waving of heteroatom I, III, V, VII and II. IV, VI, VIII cycles. out-of-phase, out-of-plane
				178.8	0.1	$2.1{\cdot}10^{-3}$		
				173.4	1.5	$3.4{\cdot}10^{-2}$		
				173.3	0.7	$1.6{\cdot}10^{-2}$		
ν_{5} e_{3g}	139	–	–	157.1	0.1	$2.6{\cdot}10^{-3}$	149	Waving of heteroatom III, VI, VIII and II, IV, VII cycles, out-of-phase, out-of-plane
				157.0	0.08	$2.1{\cdot}10^{-3}$		
				150.0	0.007	$2.0{\cdot}10^{-4}$		
				149.6	0.02	$5.8{\cdot}10^{-4}$		

(*continued on next page*)

Table 3 (*continued*)

Molecule 8S				Tetramer			Freq. exp.	Assignment
Mode	Freq. cal.	S_i	I_R	Freq. cal.	S_i	I_R		
ν_4 e_{3g}	139	–	–	146.5 146.1 143.2 142.8	3.1 0.3 2.3 0.5	$9.3\cdot10^{-2}$ $9.0\cdot10^{-3}$ $7.1\cdot10^{-2}$ $1.6\cdot10^{-2}$	149	Waving of heteroatom I, IV, VI and II, V, VII cycles, out-of-phase, out-of-plane

Freq., frequency (cm^{-1}); S_i, Raman activity, $Å^4$/amu; I_R, relative Raman intensity; cal., calculated; exp., experimental; def., deformation; s, symmetric; as, asymmetric; I–VIII, heterocycle numbers (see Fig. 1); bend., bending; str., stretching; COT, cyclooctatetraene; w, white modification of octathia[8]circulene (amorphous).

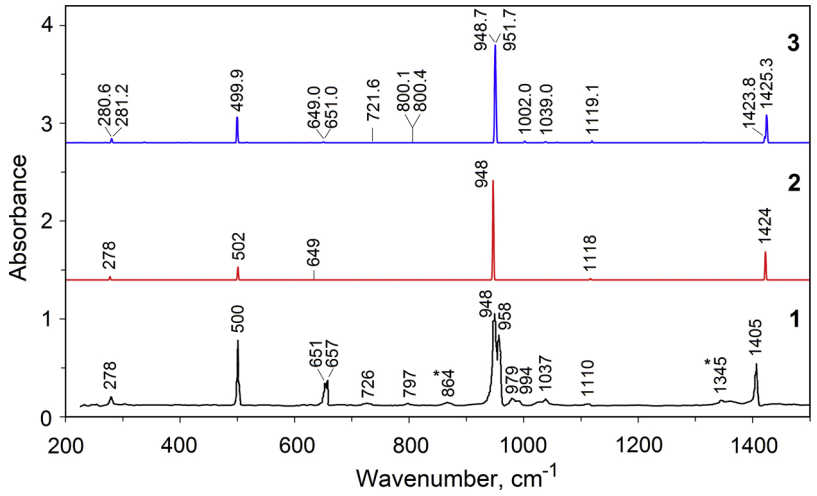

Fig. 3. Experimental IR spectrum of a red sample of compound **8S** (curve 1 [12]) in comparison with that calculated for the free molecule **8S** (curve 2) and tetramer (curve 3).

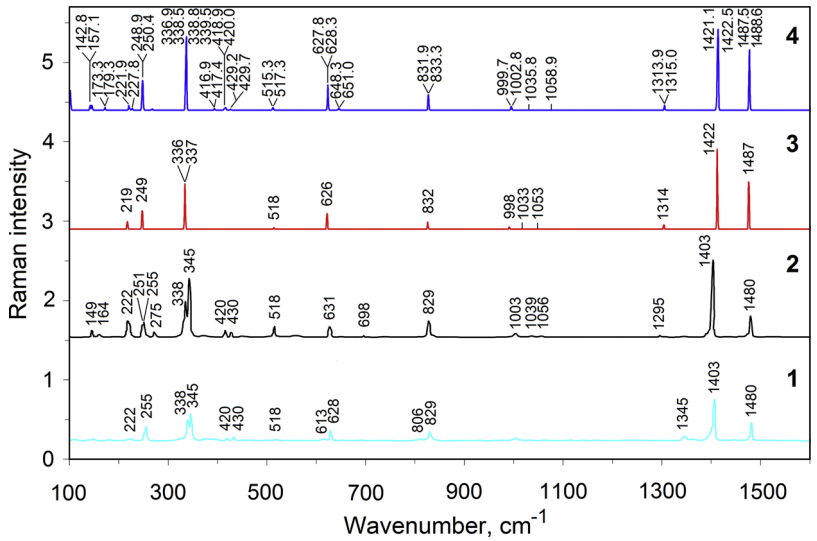

Fig. 4. Experimental Raman spectra of the white (curve 1 [12]) and red (curve 2 [12]) modification samples of compound **8S** in comparison with those calculated for the free molecule (curve 3) and tetramer (curve 4).

sublimed substance, respectively [12]. The white, cotton-like sample, contains fewer lines than the crystalline red tiny needles in Raman spectra (Fig. 4, curves 1 and 2). One should note specially the line 1345 cm^{-1} of the white sample, which is shifted by 50 cm^{-1} from the line 1295 cm^{-1} of the red crystal sample. According to our calculations we assign the last line to the mixed vibrations of the side C-C bonds and CSC angles of thiophene fragments with an intermediate frequency 1314 cm^{-1}.

The most active in Raman spectra are vibrations ν_{56} and ν_{20} of the a_{1g} symmetry with the calculated frequency 1422 and 337 cm^{-1} and activity 705 and 44 A^4/amu, respectively (relative intensity 1.0 and 0.4, Table 3, Fig. 4, curve 3). They are symmetric $C^{\alpha}C^{\beta}$ and $C^{\alpha}C^{\beta}$' stretching vibrations, occurring in-phase in all thiophene fragments (ν_{56}), and "breathing" or "pulsation" of the whole macrocycle (ν_{20}). In the experimental Raman spectrum of the red octathia[8]circulene crystal they are identified as the lines 1403 and 345 cm^{-1} (Fig. 4, curve 2). In the

observed Raman spectrum the line 345 cm^{-1} seems to be split but this splitting is produced by an overlap with the near-by line 338 cm^{-1} (normal vibration $\nu_{19(18)}$ with the calculated frequency 336 cm^{-1}).

Comparison with the tetramer calculation (Table 3) indicates that the internal splitting of each mode is negligible (about 0.3–0.8 cm^{-1}), but intermolecular interactions leads to a great increase of the Raman activity (especially for the line ν_{20}) in a total agreement with the whole observed spectrum (Fig. 4).

The normal vibration ν_{43} ("breathing" of the octatetraene cycle) also belongs to the a_{1g} symmetry, but exhibits much lower Raman activity (the relative intensity is 0.09). In the experimental Raman spectrum of the octathia[8]circulene crystal it is identified as the line 829 cm^{-1} (calc. 832 cm^{-1}) with the middle intensity because of intermolecular enhancement (Table 3, Fig. 4). We have a problem with the experimental line 1480 cm^{-1} (Fig. 4, curve 2) which belongs to out-of-phase $C^{\beta}C^{\beta'}$ stretching vibrations. The calculated intensity of this line is much higher in comparison with experiment (Fig. 4, curves 2, 3). Assignment of all experimental lines in Raman spectra of the octathia[8]circulene is given in Table 3.

3.2.3. Vibrations of low activity in Raman spectrum

Weak Raman bands in the spectrum of **8S** molecule are also interesting. Thus, the doubly degenerate modes of the e_{2g} symmetry, $\nu_{55(54)}$ and $\nu_{47}(\nu_{46})$, with the calculated frequency 1314 and 998 cm^{-1} (exp. 1295 and 1003 cm^{-1}, respectively) belong to vibrations of the shortest side C—C bonds of thiophene fragments which are mixed with the bending vibrations of the $C^{\alpha}SC^{\alpha'}$ angle. The first mode (1314 cm^{-1}) shows moderate activity inside free molecule (2·17 $Å^4$/amu, Table 3). It is split into two sub-bands with negligible frequency splitting in the tetramer, but activity of the first sub-band (ν_{55}) in the tetramer is much higher than in the second sub-band (ν_{54}, Table 3). Thus, we predict a sharp narrow line (1295 cm^{-1}) in agreement with the observed Raman spectrum.

Less active are doubly degenerate modes of the e_{1g} symmetry, $\nu_{29(28)}$ and $\nu_9(\nu_8)$, with the calculated frequency of 518 and 219 cm^{-1}, respectively. They are formed by non-planar waving vibrations of thiophene fragments. In the experimental spectrum they produce lines 518 cm^{-1} and 222 cm^{-1}, respectively, with intensity close to the middle one. This is explained by intermolecular interaction in the tetramer which provides definite enhancement of the Raman activity for particular components (Table 3, Fig. 4, curves 3, 4).

The weakly split lines 631/628 and 255/251 cm^{-1} in the observed Raman spectrum of the red crystal were detected with high resolution (Fig. 10 of Ref. [12]); we assign these lines to the planar deformations of the octatetraene cycle. In the calculated Raman spectrum of the free **8S** molecule these lines correspond to the doubly degenerate modes of the e_{2g} symmetry, $\nu_{33(32)}$ and $\nu_{13}(\nu_{12})$, with the calculated frequency 626 and 249 cm^{-1}. In the tetramer Raman spectrum their activity is increased and the splitting achieves 1–1.5 cm^{-1} (Table 3) in a reasonable agreement with observation. Tetramer calculation predicts the larger splitting of the 255/251 cm^{-1} band with non-equal intensity distribution, while the 628 cm^{-1} band splitting is produced by entire ν_{33} mode with large and equally distributed intensity whereas the former degenerate counterpart ν_{32} mode is completely quenched in the tetramer.

Assignment of the experimental lines 1594, 1056, 1039, 698, 430, 420, 417, 275, 164 and 149 cm^{-1} in the Raman spectrum of the octathia[8]circulene red crystal (Fig. 4, curve 2) can be done only on the ground of the tetramer calculation, since the normal vibrations corresponding to these frequencies $\nu_{65(64)}$ e_{3u}, ν_{51} b_{2g}, $\nu_{50(49)}$ e_{3u}, $\nu_{37(36)}$ e_{3g}, ν_{26} b_{2g}, ν_{25} b_{1g}, $\nu_{24(23)}$ e_{3u}, $\nu_{15(14)}$ e_{2u}, ν_6 b_{1u} and $\nu_{5(4)}$ e_{3g}, are symmetry forbidden in the Raman spectrum of the free **8S** molecule according to selection rules for the D_{8h} symmetry (Tables 1 and 3). In the tetramer Raman spectrum these vibrations are weakly allowed.

Raman activity of the red crystal in the region 420–430 cm^{-1} is the most interesting; it is not displayed in the free molecule calculation (Fig. 4). The ν_{26} mode of the b_{2g} symmetry formed by the $C^{\alpha}SC^{\alpha'}$ bending vibrations in the Raman spectrum of the tetramer is shifted to the observed crystal frequency (429.7 cm^{-1}) and split by 0.6 cm^{-1}. Though this splitting is a bit smaller than the observed one, the general trend of this weak (430 cm^{-1}) band occurrence can be proper explained on the ground of tetramer calculation (including its shoulder described in Ref. [12]).

The experimental split band 420/417 cm^{-1} (Fig. 10 in Ref. [12]) is formed by planar vibrations of different types; rocking of heteroatoms and bending vibrations of the $C^{\alpha}SC^{\alpha'}$ angle, respectively. This corresponds to ν_{25} b_{1g} and $\nu_{24(23)}$ e_{3u}, modes of free molecule (Table 3). The high-frequency component (ν_{25} b_{1g}) is strongly shifted to 420 cm^{-1} and occurs more active then the e_{3u}, modes at 417 cm^{-1} (ν_{24}); the former degenerate ν_{23} sub-band is fully quenched at the same time (Table 3). These fine features of the crystal-field induced Raman activity are well reproduced in the tetramer DFT simulation.

4. Conclusions

The presented and previous [14–18] DFT calculations predict that the free octathia[8]circulene molecule in a gas phase possesses a planar structure and belongs to the D_{8h} symmetry point group. Experimental IR and Raman spectra of **8S** solid exhibit numerous deviations from the characteristic selection rules of the D_{8h} point group. The perfect **8S** single crystal has a red color because of the strong intermolecular S—S interactions in the crystal packing [19]; thus, the genuine space point group of the **8S** molecule is reduced to the lower C_i symmetry which provides more complicated vibrational spectra of the crystal sample in comparison with vacuum model [12]. In the present study we have simulated the **8S** crystal packing by DFT geometry optimization of the tetramer structure preliminary obtained from the X-ray diffraction analysis. Account of dispersion correction for the B3LYP functional is shown to be useful for reproduction of the crystal-field induced deviations in IR and Raman spectra of solid red sample. Though the calculated crystal-field splitting in vibrational spectra is generally underestimated, the qualitative trends in intensity redistribution are well seeing for numerous shoulders, band shifts and broadenings. Complete assignments of all active vibrational bands in the crystal spectra permit us definitely to exclude two weak bands at 1345 and 864 cm^{-1} (marked with asterisks in Fig. 3) from IR spectrum of octathia[8]circulene sample; they are most likely due to insufficient purification.

Thus, the tetramer simulation of crystal packing reproduces many fine-structure details in the octathia[8]circulene red species and affords assignment of vibrational IR and Raman spectra.

Conflicts of interest

There are no conflicts to declare.

Acknowledgements

This work was supported by the Ministry of Education and Science of Ukraine (projects nos. 0117U003908 and 0118U003862) and the Carl Tryggers Foundation (Grant No. CTS 17:514). The calculations were supported by the Swedish National Infrastructure for Computing (SNIC) and were performed at the Parallel Data Center (PDC) within the project “Multiphysical Simulation of Molecular Materials” SNIC 020/11-23.

Appendix A. Supplementary data

Supplementary material related to this article can be found, in the online version, at doi:https://doi.org/10.1016/j.vibspec.2018.11.006.

References

[1] H.W. Kroto, J.R. Heath, S.C. O'Brien, R.F. Curl, R.E. Smalley, C_{60}: buckminsterfullerene, Nature 318 (1985) 162–163, https://doi.org/10.1038/318162a0.
[2] E. Osawa, Superaromaticity, Kagaku (Kyoto) 25 (1970) 854–863.
[3] B. Halford, The world according to Rick, Chem. Eng. News 84 (2006) 13–19.
[4] D.A. Bochvar, E.G. Galpern, On hypothetical systems: carbon dodecahedron, S-icosahedron and carbon-S-icosahedron, Dokl. Akad. Nauk SSSR (in Russian) 209 (1973) 610–612.
[5] V.N. Popov, Carbon nanotubes: properties and application, Mater. Sci. Eng. R 43 (2004) 61–102, https://doi.org/10.1016/j.mser.2003.10.001.
[6] I.V. Zaporotskova, N.P. Boroznina, Y.N. Parkhomenko, L.V. Kozhitov, Carbon nanotubes: sensor properties. A review, Modern Electron. Mater. 2 (2016) 95–105, https://doi.org/10.1016/j.moem.2017.02.002.
[7] M.S. Dresselhaus, G. Dresselhaus, P. Avouris, Carbon Nanotubes: Synthesis, Structure, Properties, and Application, Springer-Verlag, 2000 p. 464.
[8] G.V. Baryshnikov, B.F. Minaev, V.A. Minaeva, Electronic structure, aromaticity and spectra of hetero[8]circulenes, Russ. Chem. Rev. 84 (2015) 455–484, https://doi.org/10.1070/RCR4445.
[9] T. Hensel, N.N. Andersen, M. Plesner, M. Pittelkow, Synthesis of heterocyclic [8]circulenes and related structures, Synlett 27 (2016) 498–525, https://doi.org/10.1055/s-0035-1560524.
[10] N.N. Karaush, G.V. Baryshnikov, V.A. Minaeva, H. Ågren, B.F. Minaev, Recent progress in quantum chemistry of hetero[8]circulenes, Mol. Phys. 115 (2017) 2218–2230, https://doi.org/10.1080/00268976.2017.1287438.
[11] K.Y. Chernichenko, V.V. Sumerin, R.V. Shpanchenko, E.S. Balenkova, V.G. Nenajdenko, "Sulflower": a new form of carbon sulfide, Angew. Chem. 45 (2006) 7367–7370, https://doi.org/10.1002/anie.200602190.
[12] S.S. Bukalov, L.A. Leites, K.A. Lyssenko, R.R. Aysin, A.A. Korlyukov, J.V. Zubavichus, K.Yu. Chernichenko, E.S. Balenkova, V.G. Nenajdenko, M.Yu. Antipin, Two modifications formed by "sulflower" $C_{16}S_8$ molecules, their study by XRD and optical spectroscopy (Raman, IR, UV–vis) methods, J. Phys. Chem. A 112 (2008) 10949–10961, https://doi.org/10.1021/jp806134u.
[13] K.Y. Chernichenko, E.S. Balenkova, V.G. Nenajdenko, From thiophene to sulflower, Mendeleev Commun. 18 (2008) 171–179, https://doi.org/10.1016/j.mencom.2008.07.001.
[14] A. Datta, S.K. Pati, Large carrier mobilities in octathio[8]circulene crystals: a theoretical study, J. Phys. Chem. C 111 (2007), https://doi.org/10.1039/b901014a 4487–4361.
[15] G. Gahungu, J. Zhang, T. Barancira, Charge transport parameters and structural and electronic properties of octathio[8]circulene and its plate-like derivatives, J. Phys. Chem. A 113 (2009) 255–262, https://doi.org/10.1021/jp804986b.
[16] J. Aragó, P.M. Viruela, E. Ortí, From linear quaterthiophene to sulflower: a comparative theoretical study, J. Mol. Struct. (THEOCHEM) 912 (2009) 27–31, https://doi.org/10.1016/j.theochem.2009.03.021.
[17] N.N. Karaush, B.F. Minaev, G.V. Baryshnikov, V.A. Minaeva, A comparative study of the electronic structure and spectra of tetraoxa[8]circulene and octathio[8]circulene, Opt. Spectrosc. 116 (2014) 33–46, https://doi.org/10.1134/S0030400X13120084.
[18] J.H. Dopper, F.H. Wynberg, Synthesis and properties of some heterocirculenes, J. Org. Chem. 40 (1975) 1957–1966, https://doi.org/10.1021/jo00901a019.
[19] G.V. Baryshnikov, B.F. Minaev, V.A. Minaeva, V.G. Nenajdenko, Single crystal architecture and absorption spectra of octathio[8]circulene and sym-tetraselenatetrathio[8]circulene: QTAIM and TD-DFT approach, J. Mol. Model. 19 (2013) 4511–4519, https://doi.org/10.1007/s00894-013-1962-1.
[20] T. Fujimoto, M.M. Matsushita, H. Yoshikawa, K. Awaga, Electrochemical and electrochromic properties of octathio[8]circulene thin films in ionic liquids, J. Am. Chem. Soc. 130 (2008) 15790–15791, https://doi.org/10.1021/ja8072066.
[21] G. Gahungu, J. Zhang, Shedding light on octathio[8]circulene and some of its plate-like derivatives, Phys. Chem. Chem. Phys. 10 (2008) 1743–1747, https://doi.org/10.1039/b800685g.
[22] A. Dadvand, F. Cicoira, K.Yu. Chernichenko, E.S. Balenkova, R.M. Osuna, F. Rosei, V.G. Nenajdenko, D.F. Perepichka, Heterocirculenes as a new class of organic semiconductors, Chem. Commun. (2008) 5354–5356, https://doi.org/10.1039/b809259a.
[23] O. Ivasenko, J.M. MacLeod, K.Yu. Chernichenko, E.S. Balenkova, R.V. Shpanchenko, V.G. Nenajdenko, F. Rosei, D.F. Perepichka, Supramolecular assembly of heterocirculenes in 2D and 3D, Chem. Commun. (2009) 1192–1194, https://doi.org/10.1039/b819532c.
[24] T. Fujimoto, M.M. Matsushita, K. Awaga, Electrochemical field-effect transistors of octathio[8]circulene robust thin films with ionic liquids, Chem. Phys. Lett. 483 (2009) 81–83, https://doi.org/10.1016/j.cplett.2009.10.050.
[25] X.-D. Tang, Y. Liao, H.-Z. Gao, Y. Geng, Z.-M. Su, Theoretical study of the bridging effect on the charge carrier transport properties of cyclooctatetrathiophene and its derivatives, J. Mater. Chem. 22 (2012) 6907–6918, https://doi.org/10.1039/C2JM14871D.
[26] T. Fujimoto, M.M. Matsushita, K. Awaga, Dual-gate field-effect transistors of octathio[8]circulene thin-films with ionic liquid and SiO_2 gate dielectrics, Appl. Phys. Lett. 97 (2010) 123303–123306, https://doi.org/10.1063/1.3491807.
[27] C.B. Nielsen, T. Brock-Nannestad, T.K. Reenberg, P. Hammershøj, J.B. Christensen, J.W. Stouwdam, M. Pittelkow, Organic light-emitting diodes from symmetrical and unsymmetrical pi-extended tetraoxa[8]circulenes, Chem. – Eur. J. 16 (2010) 13030–13034, https://doi.org/10.1002/chem.201002261.
[28] G.V. Baryshnikov, R.R. Valiev, N.N. Karaush, V.A. Minaeva, A.N. Sinelnikov, S.K. Pedersen, M. Pittelkow, B.F. Minaev, H. Ågren, Benzoannelated aza-, oxa- and azaoxa[8]circulenes as promising blue organic emitters, Phys. Chem. Chem. Phys. 18 (2016) 28040–28051, https://doi.org/10.1039/c6cp03060b.
[29] K.B. Ivaniuk, G.V. Baryshnikov, P.Y. Stakhira, S.K. Pedersen, M. Pittelkow, A. Lazauskas, D. Volyniuk, J.V. Grazulevicius, B.F. Minaev, H. Ågren, New WOLEDs based on π-extended azatrioxa[8]circulenes, J. Mater. Chem. C 5 (2017) 4123–4128, https://doi.org/10.1039/C7TC00655A.
[30] A.D. Becke, Density-functional thermochemistry. III. The role of exact exchange, J. Chem. Phys. 98 (1993) 5648–5652, https://doi.org/10.1063/1.464913.
[31] C. Lee, W. Yang, R.G. Parr, Development of the Colle-Salvetti correlation-energy formula into a functional of the electron density, Phys. Rev. B 37 (1988) 785–789, https://doi.org/10.1103/PhysRevB.37.785.
[32] K. Raghavachari, J.S. Binkley, R. Seeger, J.A. Pople, Self-consistent molecular orbital methods. XX. A basis set for correlated wave functions, J. Chem. Phys. 72 (1980) 650–654, https://doi.org/10.1063/1.438955.
[33] A.D. Becke, Perspective: fifty years of density-functional theory in chemical physics, J. Chem. Phys. 140 (2014) 18A301, , https://doi.org/10.1063/1.4869598.
[34] N. Mardirossian, M. Head-Gordon, Thirty years of density functional theory in computational chemistry: an overview and extensive assessment of 200 density functionals, Mol. Phys. 115 (2017) 2315–2372, https://doi.org/10.1080/00268976.2017.1333644.
[35] M.J. Frisch, G.W. Trucks, H.B. Schlegel, G.E. Scuseria, M.A. Robb, et al., Gaussian 16, Revision A.03, Gaussian, Inc., Wallingford CT, 2016.
[36] P.L. Polavarapu, Ab initio vibrational Raman and Raman optical activity spectra, J. Phys. Chem. 94 (1990) 8106–8112, https://doi.org/10.1021/j100384a024.
[37] S.I. Gorelsky, SWizard Program, University of Ottawa, Ottawa, Canada, 2013http://www.sg-chem.net.
[38] S. Grimme, J. Antony, S. Ehrlich, H. Krieg, A consistent and accurate ab initio parametrization of density functional dispersion correction (DFT-D) for the 94 elements H-Pu, J. Chem. Phys. 132 (2010) 154104–154123, https://doi.org/10.1063/1.3382344.
[39] S. Ehrlich, J. Moellmann, S. Grimme, Dispersion-corrected density functional theory for aromatic interactions in complex systems, Acc. Chem. Res. 46 (2013) 916–926, https://doi.org/10.1021/ar3000844.
[40] G.V. Baryshnikov, R.R. Valiev, N.N. Karaush, B.F. Minaev, Aromaticity of the planar hetero[8]circulenes and their doubly charged ions: NICS and GIMIC characterization, Phys. Chem. Chem. Phys. 16 (2014) 15367–15374, https://doi.org/10.1039/c4cp00860j.
[41] P. Dawson, Dipole dipole interactions and Davydov splitting in crystals, J. Phys. Chem. Solids 36 (1975) 1401–1403, https://doi.org/10.1016/0022-3697(75)90223-1.